07.1

Schottky barrier in Si−M structures of solid−state lithium−ion batteries

© *A.S. Rudy, A.A. Mironenko, V.V. Naumov, A.B. Churilov*

Valiev Institute of Physics and Technology of RAS, Yaroslavl Branch, Yaroslavl, Russia
E-mail: rudy@uniyar.ac.ru

The results of measuring the charge−discharge characteristics of solid−state thin−film lithium−ion batteries with a nanocomposite anode based on the a-Si(Al) solid solution are presented. The charging characteristics of batteries have a feature in the form of a step on the gentle branch of the $U(t)$ curve. It has been suggested and substantiated that the appearance of the step is related to the gradual compensation and change of the a-Si(Al) hole conductivity to electronic one as the lithium concentration increases. As a result, the a-Si(Al)—Ti ohmic contact becomes rectifying, and the electrons participating in the Faraday process have to overcome the Schottky barrier. The potential growth required to maintain the galvanostatic charge regime manifests itself as a step on the charge curve.

Silicon is regarded as the most promising material for thin film solid−state lithium−ion batteries (SSLIBs). This is caused by a number of factors, the basic of which are high theoretical capacity (up to $4200\,\text{mA}\cdot\text{h/g}$), relatively high diffusion coefficient of lithium, and, mainly, the compatibility of the silicon application technique with the micro- and nanoelectronics technologies. However, the main advantage of crystalline silicon, namely, the ability to reversibly attach up to four lithium atoms per atom, leads to instability of battery structures. Long before such a high lithium concentration in crystalline silicon is reached, stresses able to destruct the electrode get developed. This problem was solved by using amorphous silicon with artificially restricting its capacity by its partial oxidation and increasing its conductivity by implanting $10-15$ at.% of aluminum into the silicon matrix. Finally, a magnetron sputtering technique for deposition the electrode nanocomposite material Si@O@Al was developed [1–3]; having a high capacity (up to $3000\,\text{mA}\cdot\text{h/g}$), this material withstands within TSLIB more than 1000 charge−discharge cycles.

In testing Si@O@Al−based SSLIBs, e.g., Ti–V$_2$O$_5$–LiPON–Si@O@Al–Ti, charging curves exhibited steps (Fig. 1, a) that are commonly referred to as hikes [4]. In the liquid−electrolyte batteries, emergence of hikes is typically caused by irreversible processes, e.g., those leading to the electrode destruction. In the case of SSLIBs, the charge−discharge processes are reversible, while the Coulomb efficiency is at least 95%, which is demonstrated by the curves presented in Fig. 1, a. Therefore, the only reasonable explanation of the step is formation of the Schottky potential barrier at the interface between the Si@O@Al nanocomposite and titanium down collector.

Exactly the same steps were observed in the charging curves plotted for the Ti–LiCoO$_2$–LiPON–Si@O@Al–Ti SSLIB structure (Fig. 1, b). Batteries based on lithium cobaltite Li$_{1-x}$CoO$_2$ work in a limited potential window of $0-3.5\,\text{V}$ which corresponds to $0 \leqslant x < 0.5$; this is why the charging curves exhibit only onsets of the steps. Restriction of the potential is connected with the fact that ordering of lithium vacancies takes place at $x > 0.5$, as a result of which cobalt irreversibly turns to the tetravalent state with formation of CoO$_2$. For this reason, the practical capacity of lithium cobaltite does not exceed a half of the theoretical one and equals $140\,\text{mA}\cdot\text{h/g}$. Comparison of the Fig. 1 curves shows that, at the almost equal parameters of the vanadium oxide batteries and somewhat higher capacity, the lithium−cobaltite battery discharge time is twice shorter since only a half of lithium gets extracted in charging.

Formation of the charging curve step is directly related with the Si@O@Al nanocomposite elemental composition comprising about 70% of silicon, 15 to 20% of oxygen and, as well, 10 to 15% of aluminum. In this case, the Si@O@Al films are X-ray amorphous and remain the same in the charge−discharge cycling process. The role of the stabilizer of the a-Si phase within the nanocomposite is played by aluminum that, being located in the lattice sites and interstitials, prevents silicon crystallization in the process of lithium extraction. In this case it is possible to regard the Si@Al system as the a-Si(Al) solid solution in which amorphous silicon is the solvent and aluminum is the solute. What is important is that the aluminum solubility under the equilibrium conditions is very low; as per various data, its maximal value is 0.016 to 0.038 at.%. A higher aluminum concentration in a-Si(Al) may be achieved by atomically mixing Si and Al in the process of the magnetron−sputtering fabrication of the film.
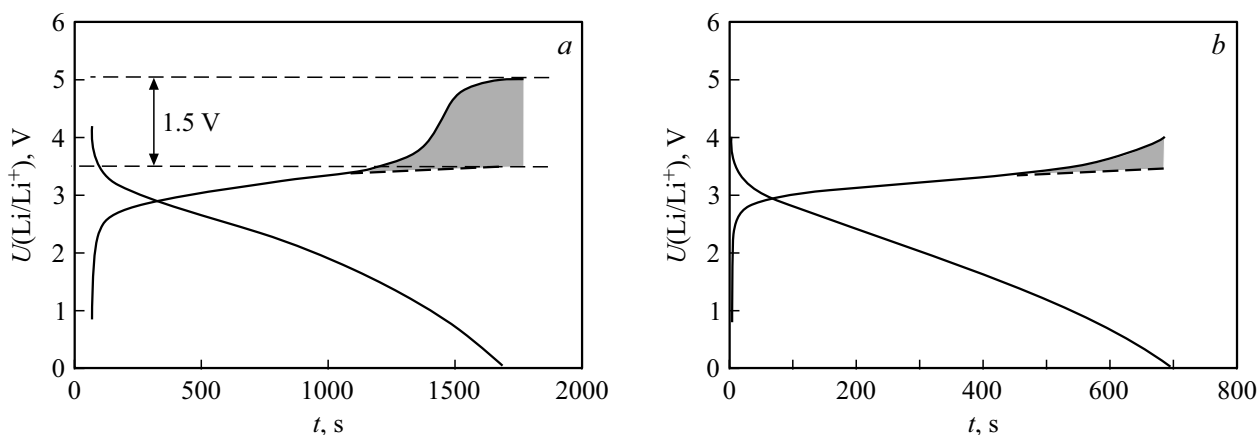
Figure 1. *a* — charge−discharge curve of the Ti—V$_2$O$_5$—LiPON—Si@O@Al—Ti SSLIB (area $S = 7.9$ cm^2, 119th cycle, potential window 0−5 V, current 100 μA); *b* — charge−discharge curve of the Ti—LiCoO$_2$—LiPON—Si@O@Al—Ti SSLIB (area $S = 7.9$ cm^2, 76th cycle, potential window 0−4 V, current 100 μA).
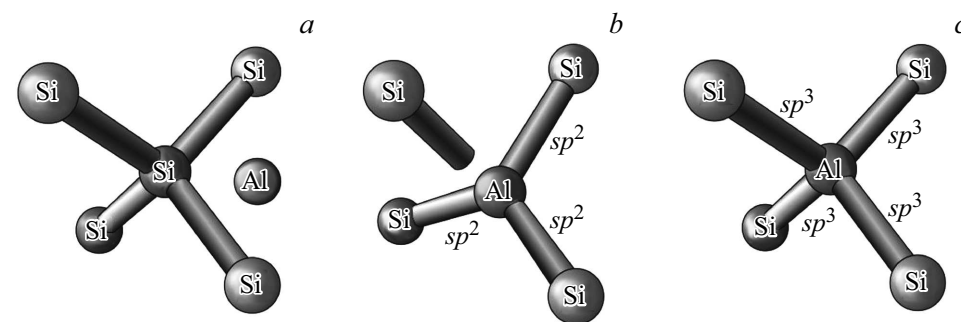

Figure 2. Possible variants for implanting aluminum into the silicon crystal lattice.

When silicon is deposited on a cold substrate, an amorphous a-Si(Al) structure is formed, where aluminum can take positions as shown in Fig. 2. For instance, Al can take interstitial position in the crystal lattice without forming a chemical bond with Si (Fig. 2, *a*). In this case, a-Si(Al) is the interstitial solid solution. Theoretically, sp^2-hybridized Al can form in a severely distorted crystal lattice a compound with silicon shown in Fig. 2, *b*; however, there are no any experimental confirmations for the existence of such compounds. Most probable is the excited sp^3-hybridized state of Al in which the bonds are directed to the tetrahedron apexes; this allows Al to integrate into the silicon crystal lattice with minimal distortions of the latter (Fig. 2, *c*). The electron lacking for this is to be captured from the orbital of the nearest silicon atom; as a result, a hole emerges in the a-Si(Al) valence band. Thus, the sp^3-hybridized aluminum is at the same time an acceptor impurity, while a-Si(Al) is the substitutional solid solution. In addition, during Si@O@Al deposition there arise small amounts of kaolinite Al$_4$[Si$_4$O$_{10}$](OH)$_8$, sillimanite (Al$_2$O$_3$)(SiO$_2$), and, separately, nanocrystalline Al$_2$O$_3$ and amorphous silicon dioxide SiO$_2$; this is shown by the data of X-ray phase analysis and Raman−scattering spectroscopy. These dielectric and chemically inert compounds do not affect, to any extent, the a-Si(Al) band structure. At the same time, they play a role of the structure „disintegrator" since they raise the number of defects, pores and grain boundaries, which increases the lithium diffusivity.

Being for silicon an acceptor impurity [5], sp^3-hybridized Al significantly increases the valence−band hole concentration. According to direct measurements, the Si@O@Al conductivity is $\sigma = 3.19 \cdot 10^{-4}$ S · m^{-1}, which gives $n\mu = 1.99 \cdot 10^{15}$ S · m^{-1} · C^{-1}; this means that, when the hole concentration is $n \sim 10^{-21}$ m^{-3}, i. e., the maximum possible concentration for non−degenerate semiconductors, mobility is $\mu \sim 10^{-6}$ m^2/(V · s) that is two orders of magnitude higher than the a-Si charge carrier mobility. High concentration of the sp^3-hybridized Al and high hole mobility imply low localized state density which, similarly to that in hydrogenated silicon a-Si:H, may be about $10^{15}-10^{16}$ eV^{-1} · cm^{-3}. Therefore, hereinafter we assume that the Fermi level is not fixed and shifts during lithiation in accordance with the occupation of the Al and Li impurity levels [5], i. e., from the valence band top to the conductivity band bottom (Fig. 3).

The conductivity band and valence band boundaries in the band diagram presented in Fig. 3 are located at −2.3 and −3.5 eV, respectively. These values are taken from paper [6]
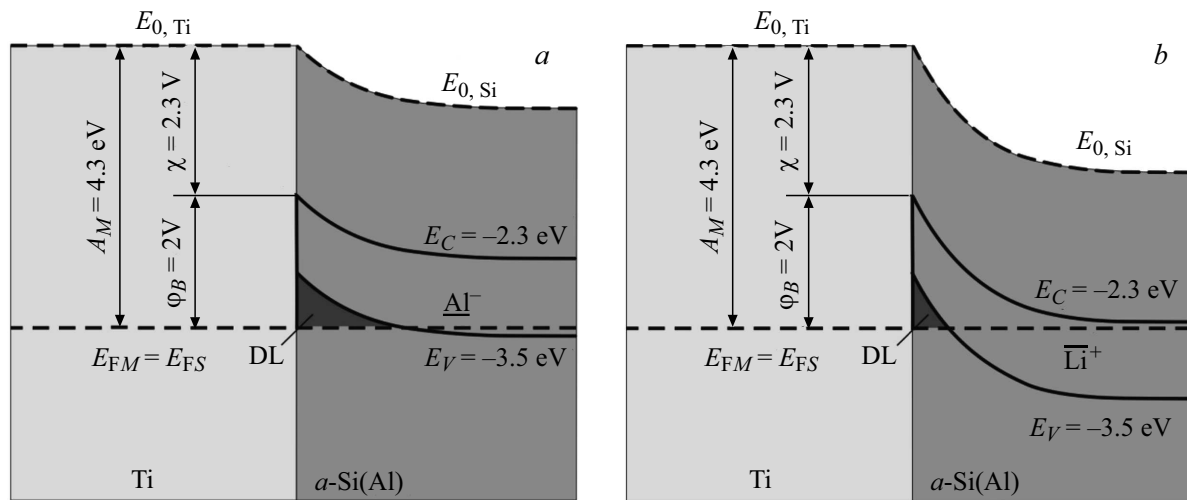
Figure 3. Band structure of the *a*-Si(Al)−Ti contact. *a* — non−lithiated (hole−type) *a*-Si(Al); *b* — lithiated (electron−type) *a*-Si(Al). A_M is the titanium work function, χ is the electron affinity, E_{FM} is the titanium Fermi level, E_{FS} is the amorphous silicon Fermi level, E_C, E_V is the mobility−threshold energy (relative to vacuum), DL is the degenerate layer.

that presents calculations of the band tail states obtained by using a large and realistic *a*-Si model comprising 4096 atoms (a cube with the side of about 43 Å). Exactly the same results were obtained in [7] by the method described in [8]. The use of the results of studies [6,7] where dissolved components were ignored is quite permissible because the amorphous silicon band diagram is defined by the crystal lattice short−range ordering that does not change after Al implantation (Fig. 2, *a, c*). The dissolved components may affect only the localized state density and charge carrier concentration. For instance, the sp^3-hybridized aluminum, unlike hydrogen in hydrogenated silicon, not only reduces the localized state density but also increases the hole concentration. The titanium work function indicated in Fig. 3 is the mean value of experimental data ranging from 4.14 to 4.54 eV. Such a data spread is caused by the work function dependence on the surface purity. As shown in Fig. 3, the Fermi level matches with the mean work function of 4.3 eV.

Formation of the Schottky barrier in the vicinity of the Si@O@Al—Ti contact may be qualitatively explained as follows. When the lithium concentration is low, *a*-Si is a *p*-type semiconductor, and its contact with Ti is ohmic and forward−biased. On the side of semiconductor, charge carriers of two types pass through the contact: holes and lithium ions recombining with electrons at the boundary. The hole current in a *p*-semiconductor prevails over the ion current in which electrons have to overcome the potential barrier and, hence, voltage drop at the contact is small, and the charging curve is free of the step. During the Si@O@Al nanocomposite lithiation, gradual compensation of the *a*-Si(Al) semiconductor takes place, which is followed by the conductivity type hole−to−electron conversion. The *a*-Si−Ti contact becomes rectifying and reverse−biased (with „minus" at the metal). In this case, the main contribution

to the current through the contact comes from the ion conductivity, while electrons recombining with lithium ions have to overcome the Schottky barrier on the side of metal. To keep the current constant during charging, the galvanostat increases the voltage by the value of the Schottky barrier height, which results in appearance of the step in the charging curve. Notice that the Schottky barrier height on the side of metal is $\varphi_B = A_M - q\chi$ where χ is the electron affinity independent of the semiconductor Fermi level; therefore, the gradual appearance of the barrier in the form of the step is caused only by conversion of the *a*-Si conductivity. When the titanium work function is 4.3 eV and electron affinity is $\chi = 2.3$ V, the barrier height should be 2 V.

The step height in Fig. 1, *a* is 1.5 V which is 0.5 V lower than the height of the Schottky barrier shown in the band diagram (Fig. 3). The most probable reason for the barrier lowering may be the Schottky effect caused by the electrical image forces, existence of surface states on the amorphous silicon surface, and double electric layer. When the diffusion coefficient of lithium ions is $D = 5 \cdot 10^{-10}$ cm^2/s, their mobility is $\mu = 1.9 \cdot 10^{-8}$ cm^2/(V · s) and is comparable with the charge carrier mobility in amorphous silicon. During charging, lithium ions create something similar to the double electric layer in the region of spatial charge thus changing the potential barrier height and shape. In this case, the field will be concentrated in the gap of the double electric layer, i. e., inside the depletion layer. Moreover, the width of the depletion layer in amorphous silicon depends not only on the bias voltage but also on the concentration of deep and shallow traps of the donor and acceptor types [9]. The mathematical model describing all the mentioned contributions to the potential barrier would allow making quantitative estimations and form a clear view of both the reasons for the barrier height reduction and

its shape. Nevertheless, the proposed qualitative model provides a consistent explanation for specific features of the SSLIB charging curves via the Schottky barrier creation due to the hole−type a-Si(Al) semiconductor compensation in the process of lithiation.

Financial support

Conflict of interests

The authors declare that they have no conflict of interests.

References

[1] T.L. Kulova, A.A. Mironenko, A.M. Skundin, A.S. Rudy, V.V.Naumov, D.E. Pukhov, Int. J. Electrochem. Sci., **11**, 1370 (2016).
http://www.electrochemsci.org/papers/vol11/110201370.pdf

[2] A.A. Airapetov, S.V. Vasiliev, T.L. Kulova, M.E. Lebedev, A.V. Metlitskaya, A.A. Mironenko, N.F. Nikol'skaya, V.V. Odinokov, G.Ya. Pavlov, D.E. Pukhov, A.S. Rudyi, A.M. Skundin, V.A. Sologub, I.S. Fedorov, A.B. Churilov, Russ. Microelectron., **45** (4), 285 (2016). DOI: 10.1134/S1063739716030021.

[3] A.A. Mironenko, I.S. Fedorov, A.S. Rudy, V.N. Andreev, D.Yu. Gryzlov, T.L. Kulova, A.M. Skundin, Monatsh. Chem., **150** (10), 1753 (2019). DOI: 10.1007/s00706-019-02497-1

[4] T.L. Kulova, A.A. Mironenko, A.S. Rudy, A.M. Skundin, *All solid state thin-film lithium-ion batteries: materials, technology, and diagnostics* (CRC Press, Boca Raton, 2021). DOI: 10.1201/9780429023736

[5] M. Grundmann, *The physics of semiconductors: an introduction including nanophysics and applications.* Ser. Graduate Texts in Physics (Springer, Cham, 2021). DOI: 10.1007/978-3-030-51569-0.

[6] D.A. Drabold, U. Stephan, J. Dong, S.M. Nakhmanson, J. Mol. Graphics Mod., **17** (5-6), 285 (1999). DOI: 10.1016/S1093-3263(99)00036-4

[7] B.A. Golodenko, A.B. Golodenko, Vestn. VGUIT, № 2, 65 (2014). https://cyberleninka.ru/article/n/modelirovanie-elektronnoy- struktury-i-raschyot-osnovnyh-elektro-fizicheskih-parametrov-amorfnogo- kremniya (in Russian)

[8] B.A. Golodenko, A.B. Golodenko, Nano— i mikrosistemnaya tekhnika, № 11(148), 23 (2012). (in Russian)
http://www.microsystems.ru/files/publ/article201211p23-27.pdf

[9] S.P. Vikhrov, N.V. Vishnyakov, V.G. Mishustin, *Fizicheskie protsessy v bar'ernykh strukturakh na osnove neuporyadochennykh poluprovodnikov* (Vuzovskoe obrazovanie, Saratov, 2019). (in Russian)